Characterizations and boron diffusion modelling on the AISI H13 steel

M. Ortiz-Domínguez [a], M. Keddam [b, *], Á.J. Morales-Robles [c]

[a]Autonomous University of Hidalgo State, Escuela Superior de Ciudad Sahagún-Mechanical Engineering, Hidalgo, México

[b] Laboratory of Materials Technology, Faculty of Mechanical Engineering and Process Engineering, USTHB, Algiers, Algeria

[c] Autonomous University of Hidalgo State, Área Académica de Ciencias de la Tierra y Materiales- Instituto de Ciencias Básicas e Ingeniería, Hidalgo, México

*Email: keddam@yahoo.fr

(Received 23 April 2024; Accepted 19 November 2024)

Abstract

A kinetic approach accounting for the linearity of boron profiles through the boronized layer on AISI H13 steel was developed. It aims to track the temporal evolution of the thicknesses of FeB and (FeB + Fe_2B) layers by considering new expressions for the mass balance equation at each growth front. These surface layers were generated by pack-boronizing AISI H13 steel in the temperature range of 1123 to 1273 K for durations ranging from 2 to 8 h. Finally, this linear model has been validated for two other sets of processing parameters (1323 K for 4.5 and 8.5 h). Iso-thickness diagrams were also proposed to optimize the thicknesses of the layers for targeted industrial usage.

Key-words*: Boronizing, borides, diffusion model, Activation energy, contour diagram.*

1. Introduction

Boriding is a well-known surface treatment method in industrial sectors aimed at improving the surface properties of surface-hardened layers produced on various metals [1,2,3] and alloys [4,5]

, especially high-alloy steels [6,7] . This process involves heating the material within the typical temperature range of 800-1050°C for 0.5-10 h to create boron compounds with the host metal as compact layers, as well as forming precipitates inside them via the diffusion process of boron atoms resulting from a boron-rich medium. The benefits of applying the boronizing process include increasing the surface hardness of the produced layers, ensuring resistance to wear, and enhancing the ability to withstand corrosion. Many boriding methods are implemented in laboratories, but few are applicable in industrial sectors due to certain shortcomings. One can cite liquid boriding with and without electrolysis, gas boriding, plasma boriding, boriding in fluidized beds, powder or paste boriding, and pack boriding assisted with electrical fields. It is noted that powder pack boriding is the far preferred process for treating steels in accordance with industrial requirements. The AISI H13 tool steel is well-suited for use in both hot and cold work tooling. Its outstanding hot hardness provides resistance against thermal fatigue cracking, which can occur due to repetitive heating and cooling in hot work environments. With its high toughness and strong resistance to thermal fatigue cracking, the AISI H13 steel stands as the desired option for a range of hot work tooling applications. Nonetheless, to increase its surface hardness and wear resistance in extreme working conditions, experts highly recommend employing the boriding process to achieve this goal. To optimize the thickness of the layers to meet the requirements of industrial applications, modeling boriding kinetics is crucial. Therefore, various mathematical approaches have been reported in the literature to achieve this goal. These approaches include deterministic models [6, 8-13] a stochastic model [14] and non-deterministic models [15, 16].

In this study, the boride layers on AISI H13 steel were characterized through SEM observations and analyses to confirm the interphase morphology. XRD analysis was conducted to identify iron borides and metal borides. The surface hardness of the boride layers was determined through Vickers microhardness measurements to establish a microhardness profile.

Additionally, a kinetic approach known as the linear model was utilized to estimate the boron diffusion coefficients in iron borides. Boron activation energies in both phases (FeB and Fe_2B) were evaluated by determining two dimensionless constants, and then compared to values available in the literature. Finally, the linear model was verified by employing two additional processing parameters.

2. Material, boriding treatment and experimental techniques

The AISI H13 steel to be employed for boriding experiments had a nominal chemical composition (in weight percent) of 0.32-0.45% C, 0.20-0.50% Mn, 0.80-1.20% Si, 4.75-5.50% Cr, 1.10-1.75% Mo, 0.0-0.03% P, 0.0-0.03% S, 0.0-0.3% Ni, 0.0-0.25% Cu and 0.80-1.20% V. The specimens to be subject to this thermochemical treatment had a cubic shape with 10 mm side. Before the treatment, the samples were ground by employing SiC emery papers up to grit 2500 and being immersed in ultrasonic bath filled by n-heptane and ethanol for 20 min. The samples were placed inside a stainless steel container and embedded in the powder having a chemical composition of 33.5 % B_4C, 5.4 % KBF_4 and 61.1% SiC). The conventional furnace of brand Nabertherm N 250/85 HA was employed for heating the treated samples at considered temperatures for different time durations by using Argon gas as a protective atmosphere. The selected boriding temperatures were 1123 K, 1173 K, 1223 K and 1273 K for 2 h to 8 h. Once the boriding treatment was finished, the samples were taken from the furnace and kept cooled in air to ambient temperature. The cross-sections of borided samples were polished according to the standard metallographic procedure for SEM examinations with Quanta 3D FEG-FEI JSM7800-JOEL coupled with EDS analyses. To do so, the EDS system used includes the X-Max Extreme which is a silicon drift detector (SDD). It is characterized by significant enhancements in low-energy sensitivity for the detection of light elements such as boron and carbon. With X-Max Extreme, both imaging and EDS performance can be obtained simultaneously and the EDS resolution approaches that of the SEM.

The Oxford Aztec Microanalysis System was employed to collecting and analyzing the EDS results. This system includes all the hardware and software tools to perform the targeted chemical analysis. The eZAF (atomic number (Z), absorption (A) and fluorescence (F))

algorithm was used to calculate the quantity of an element detected by the software application. Matrix correction algorithms ZAF were utilized for standardless quantitative analysis in SEM-EDS analysis. The energy values of the K characteristic X-ray data of the analysed elements was presented in the spectrum. The selected parameters for EDS settings comprise the following parameters : acceleration voltage (5 or 10 eV), take-off angle(35°), live time (30 s) and resolution values. The image collected was at the specified resolution of (2024×800) with the possiblity of selecting the resolution from a drop-down list in the Settings bar.

The Nital solution of 4 vol.% was used to etch the observed surfaces. An automatized procedure for measuring the layers‘ thicknesses was carried out by using a MSQ PLUS software. Mean values of layers‘ thicknesses were obtained based on fifty measurements on the selected cross-sections of boronized samples. The identification of boride phases at the surfaces of treated samples was done by using diffractometer of brand (Equinox 2000) with Co-Kα radiation at λ_{Co} = 0.179 nm. The microhardness profile across the boronized layer was determined with a Vickers indenter under a load of 50 g and dwell time of 15 s.

3. Linear diffusion model

A recent method was proposed [9] to evaluate the boron diffusion coefficients in iron borides (FeB and Fe_2B) by applying the notion of linearity to the distribution of boron atoms through the boride layers. For this objective, new mass balance equation expressions were then developed. The time evolution of the boron distribution across the FeB and Fe_2B in a substrate that is saturated with boron atoms is seen schematically in **Figure 1**.

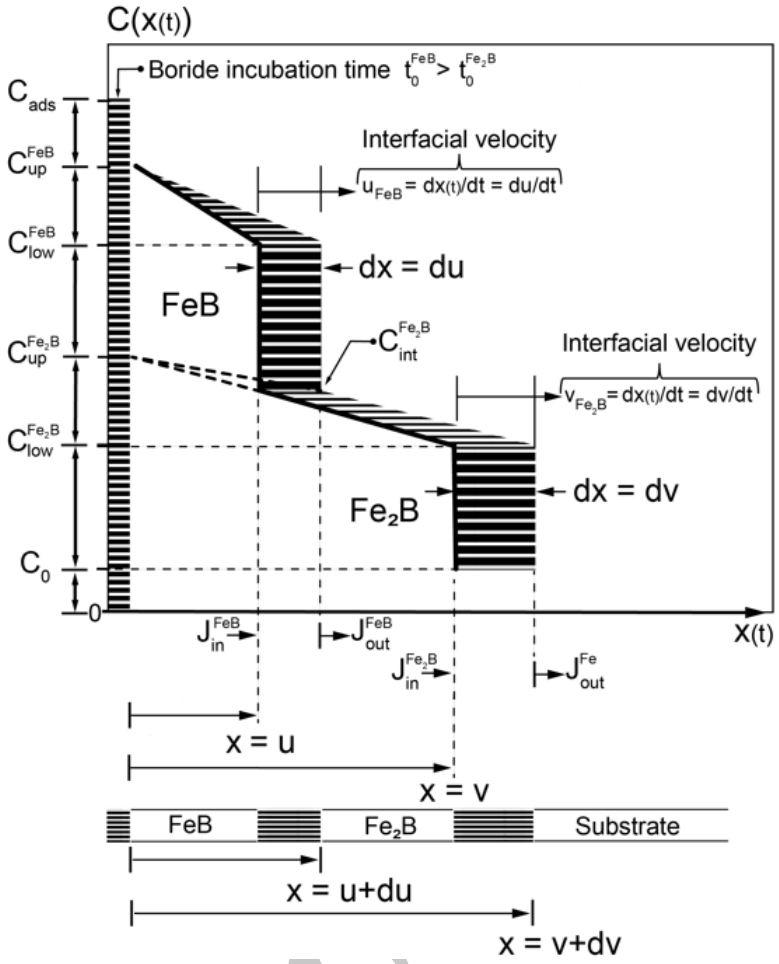

Figure 1. *Schematic depiction of linear profiles of boron element when creating the bilayer (FeB/ Fe_2B).*

The highest and lowest concentrations in FeB are shown in Figure 1 as follows: (=16.40 wt.%B) and (=16.23 wt.%B). In contrast, the equivalent maximum and minimum concentrations in the Fe_2B phase are equal to (= 9 wt.%B) and (=8.83 wt.%B) [10]. The term C_{ads} refers to the boron active adsorbed quantity as determined by Yu et al. [20]. The variable $u(t)$ represents the thickness of the FeB layer, while $v(t)$ is the bilayer (FeB/Fe_2B) thickness. C_0 indicates the boron concentration's equilibrium value inside the substrate, which is negligible [21]. Equation (1) describes the change in thickness of FeB layer expressed by:

$$u(t) = 2\varepsilon_{FeB} D_{FeB}^{1/2} \left(t - t_0^{FeB}\right)^{1/2} \quad (1)$$

With ε_{FeB} a dimensionless constant related to the diffusivity of boron in the same phase with t_0^{FeB} its corresponding incubation time. The bilayer thickness (FeB +Fe_2B) is given Equation (2):

$$\mathrm{v}(t) = 2\varepsilon_{Fe_2B} D_{Fe_2B}^{1/2} \left(t - t_0^{Fe_2B}\right)^{1/2} \quad (2)$$

With ε_{Fe_2B} a dimensionless constant and $t_0^{Fe_2B}$ the incubation time for the bilayer (FeB+ Fe_2B). This diffusion problem is subjected to the initial and boundary conditions stated as:

(at $t = 0$): $$C_i(x) = 0, \text{ for } x > 0, \textit{with } i = FeB, Fe_2B, \quad (3)$$

$$C_{FeB}(x = 0) = C_{up}^{FeB}, \text{ for } C_{ads}^{B} > 16.40\ wt.\%, \quad (4)$$

$$C_{FeB}(x = u) = C_{low}^{FeB}, \text{ for } C_{ads}^{B} < 16.23\ wt.\%, \quad (5)$$

$$C_{Fe_2B}(x = u) = C_{int}^{Fe_2B}, \text{ for } C_{ads}^{B} > 9.0\ wt.\%. \quad (6)$$

$$C_{Fe_2B}(x = \mathrm{v}) = C_{low}^{Fe_2B}, \text{ for } C_{ads}^{B} < 8.83\ wt.\%. \quad (7)$$

Let's write the mass balance equation that represents the Fe_2B layer's temporal evolution in a steady state. Equation (8) may be used to represent the boron concentration profile in the Fe_2B phase in this instance by taking into consideration the initial and boundary conditions given by Equations (6) and (7):

$$C_{Fe_2B}(x) = C_{int}^{Fe_2B} + \frac{C_{low}^{Fe_2B} - C_{int}^{Fe_2B}}{\mathrm{v} - u}(x - u). \quad (8)$$

In this case, the mass balance equation at the (Fe_2B/substrate) interface can be readily established by considering the entering mass flux of boron atoms from the side of Fe_2B phase as : $\vec{J}_{Fe_2B}[x(t)]_{x=\mathrm{v}}\,\hat{i} = -D_{Fe_2B}\left\{dC_{Fe_2B}[x(t)]/dx\right\}_{x=\mathrm{v}}\hat{i}$ and also the leaving mass of boron atoms from the Fe2B phase in the direction of the substrate flux, which is provided by: $\vec{J}_{Fe}[x(t+dt)]_{x=\mathrm{v}+d\mathrm{v}}\,\hat{i} = -D_{Fe}\left\{dC_{Fe}[x(t+dt)]/dx\right\}_{x=\mathrm{v}+d\mathrm{v}}\hat{i} = 0.$ We arrive at Equation (9) which denotes the obtained mass balance needed for determining the dimensional constant ε_{Fe_2B}:

$$\left(\frac{C_{low}^{Fe_2B}-2C_0+C_{int}^{Fe_2B}}{2}\right)\left(\frac{dx}{dt}\right)\Big|_{x=\mathrm{v}}\hat{i}=-D_{Fe_2B}\frac{dC_{Fe_2B}(x)}{dx}\Big|_{x=\mathrm{v}}\hat{i}. \quad (9)$$

Equation (10) can be easily derived by replacing the time derivative of Equation (1) and spatial derivative of Equation (8) with regards to the diffusion distance into Equation (9):

$$\left(\frac{C_{low}^{Fe_2B}-2C_0+C_{int}^{Fe_2B}}{2}\right)\frac{\varepsilon_{Fe_2B}D_{Fe_2B}^{1/2}}{\left(t-t_0^{Fe_2B}\right)^{1/2}}=-D_{Fe_2B}\left(\frac{C_{low}^{Fe_2B}-C_{int}^{Fe_2B}}{\mathrm{v}-u}\right). \quad (10)$$

By considering the equality of slopes in the Fe_2B region of Figure 3, Equation (11) can be deduced from the geometrical considerations as follows:

$$\frac{C_{low}^{Fe_2B}-C_{up}^{Fe_2B}}{\mathrm{v}}=\frac{C_{int}^{Fe_2B}-C_{up}^{Fe_2B}}{u}=\frac{C_{low}^{Fe_2B}-C_{int}^{Fe_2B}}{\mathrm{v}-u}. \quad (11)$$

Substituting the left hand-side (LHS) of Equation (11) into Equation (10), we can easily derive Equation (12) in the following form:

$$\left(\frac{C_{low}^{Fe_2B}-2C_0+C_{int}^{Fe_2B}}{2}\right)\frac{\varepsilon_{Fe_2B}}{\left(t-t_0^{Fe_2B}\right)^{1/2}}=-D_{Fe_2B}^{1/2}\left(\frac{C_{low}^{Fe_2B}-C_{up}^{Fe_2B}}{\mathrm{v}}\right). \quad (12)$$

By replacing the Equation (2) into Equation (12), we deduce the dimensionless constant ε_{Fe_2B} as follows:

$$\varepsilon_{Fe_2B}^2=\frac{(C_{up}^{Fe_2B}-C_{low}^{Fe_2B})}{(C_{low}^{Fe_2B}-2C_0+C_{int}^{Fe_2B})}. \quad (13)$$

In the same way, the mass balance equation relative to the growth of FeB layer can be found by considering the entering mass flux from the surface expressed by: $\vec{J}_{FeB}\lfloor x(t)\rfloor_{x=u}\hat{i}=-D_{FeB}\left\{dC_{FeB}\left[x(t)\right]/dx\right\}_{x=u}\hat{i}$ and the exiting mass flux towards the Fe_2B region given by: $\vec{J}_{FeB}\lfloor x(t+dt)\rfloor_{x=u+du}\hat{i}=-D_{Fe_2B}\left\{dC_{Fe_2B}\left[x(t+dt)\right]/dx\right\}_{x=u+du}\hat{i}$. Finally we arrive at the expression of Equation (14) given by:

$$\left(\frac{C_{up}^{FeB}-2C_{int}^{Fe_2B}+C_{low}^{FeB}}{2}\right)\left(\frac{dx}{dt}\right)\Big|_{x=u}\hat{i}=-D_{FeB}\frac{dC_{FeB}(x)}{dx}\Big|_{x=u}\hat{i}-\left(-D_{Fe_2B}\frac{dC_{Fe_2B}(x)}{dx}\Big|_{x=u+du}\right)\hat{i}. \quad (14)$$

Moreover, the boron concentration within the FeB layer under steady-state diffusion is expressed by Equation (15), accounting for the initial and boundary conditions provided by Equations (4) and (5).

$$C_{FeB}(x) = \frac{C_{low}^{FeB} - C_{up}^{FeB}}{u} x + C_{up}^{FeB}. \quad (15)$$

By substituting the time derivative of Equation (1) and the spatial derivatives of Equations (8) and (15) at x=u into Equation (14), we obtain Equation (16):

$$\left(\frac{C_{up}^{FeB} - 2C_{int}^{Fe_2B} + C_{low}^{FeB}}{2} \right) \left(2\varepsilon_{FeB} D_{FeB}^{1/2} \right) \hat{i} = -D_{FeB} \left(\frac{C_{low}^{FeB} - C_{up}^{FeB}}{\varepsilon_{FeB} D_{FeB}^{1/2}} \right) \hat{i} + D_{Fe_2B} \left(\frac{C_{int}^{Fe_2B} - C_{up}^{Fe_2B}}{\varepsilon_{FeB} D_{FeB}^{1/2}} \right) \hat{i}. \quad (16)$$

For the convenience, we define two slopes from Equations (1) and (2) as follows:

$$\kappa_1^2 = 4\varepsilon_{Fe_2B}^2 D_{Fe_2B}, \quad (17)$$

$$\kappa_2^2 = 4\varepsilon_{FeB}^2 D_{FeB}. \quad (18)$$

Incorporating the expressions of the two slopes κ_1^2 and κ_2^2 into Equation (16) and rearranging all terms, we can arrive at Equation (19), which provides the expression of ε_{FeB}^2:

$$\varepsilon_{FeB}^2 = \frac{\varepsilon_{Fe_2B}^2 \left(C_{up}^{FeB} - C_{low}^{FeB} \right) \kappa_2^2}{\varepsilon_{Fe_2B}^2 \left(C_{up}^{FeB} - 2C_{int}^{Fe_2B} + C_{low}^{FeB} \right) \kappa_2^2 - \kappa_1^2 \left(C_{int}^{Fe_2B} - C_{up}^{Fe_2B} \right)}. \quad (19)$$

4. Results and discussions

4.1. SEM observations of cross-sectional views of boronized layers and EDS analyses

Figure 2 displays the cross-sections of boronized layers on the AISI H13 steel obtained at different conditions. The SEM images confirm the formation of a characteristic morphology of phase interfaces marked by a low degree of columnarity ascribed to the effect of alloying elements present in the substrate as shown in a similar study [22]. In fact, for alloyed steels [23, 24], the interfaces are flattened due to the high content of Cr and Ni reducing the flux of active

boron and filling up the space in between the boride needles. Contrary, the interfaces obtained on the borided Armco iron [25] are markedly tooth shaped with needles varying in width and length due to the absence of alloying elements. In a very recent study [26], adding copper with a content of 30 wt.% in the powders mixture, has an adverse effect by suppressing the columnarity of boride needles for Armco iron and producing thicker layers. The layers' thicknesses are affected by varying the time durations from 2 to 8 h at 1273 K between 31.16 ± 8.04 and 80.05 ± 19.9 μm due to the thermal activation of boron diffusion phenomenon.

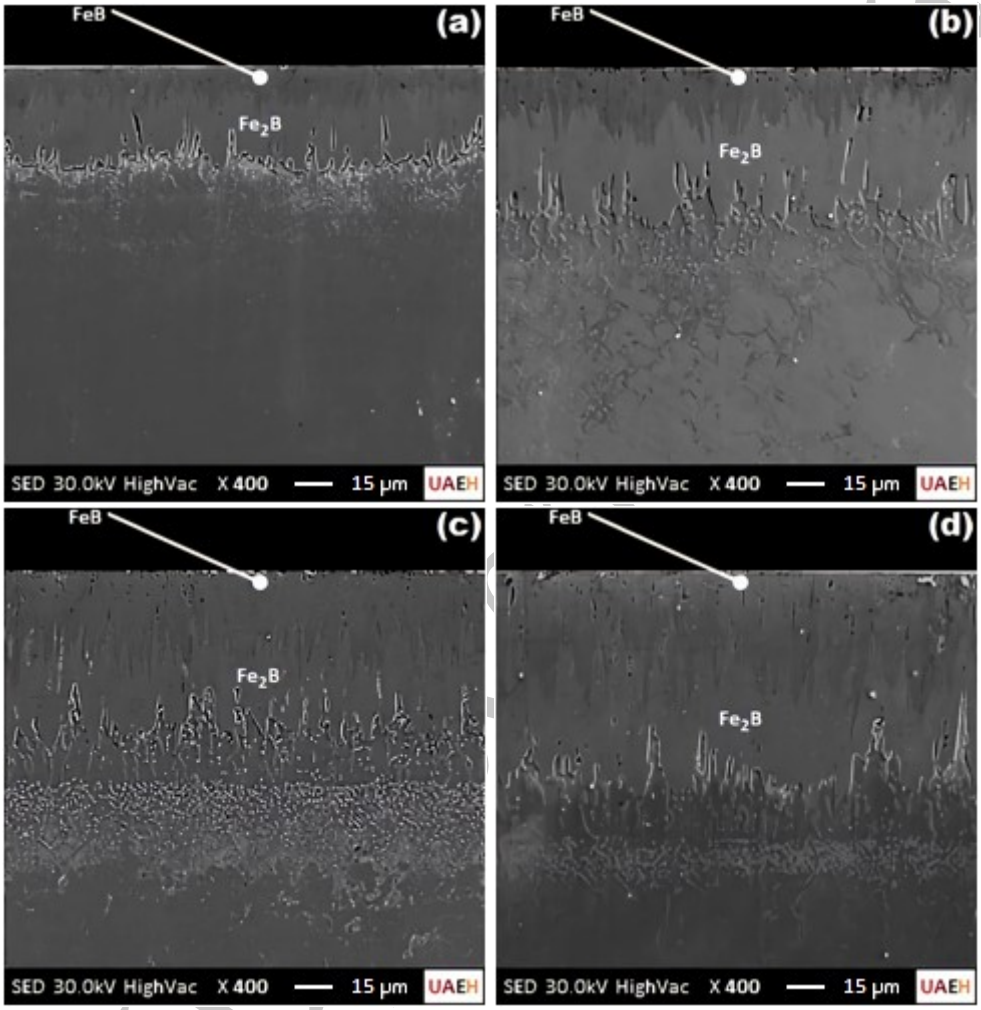

Figure 2. *SEM examinations of the cross-sections of boronized layers on AISI H13 steel at 1273 K for increasing time durations : a) 1273 K for 2 h, b) 1273 K for 4 h, c) 1273 K for 6 h and d) 1273 K for 8 h.*

It is well established that the boronizing process applied to unalloyed or low-alloyed iron-based materials forms a boride layer, which may encompass the Fe_2B or Fe_2B + FeB phase. The Fe-B phase diagram shows that the Fe_2B and FeB phases consist of approximately 8.83 wt.% and 16.23 wt.% B, respectively [9]. **Figure 3** displays the characteristic peaks from the EDS analyses taken from 2 zones (In close proximity to the upper surface and around the interface area). These analyses were performed along the cross-section of borided AISI H13 steel at 1273 K for 8 h. The qualitative peak of boron with low intensity is visible in **Figures 3a and 3b**, demonstrating a chemical reaction occurring between iron and boron to give rise to iron borides (FeB and Fe_2B) as continuous layers. The presence of alloying elements such as chromium, nickel and manganese can react chemically with the remaining boron to form precipitates of metal borides inside the boronized layer. Along the cross-section of a boronized sample at 1223 K for 10 h, the amount of element B in the boride layers was determined to be about 14.94 wt.% for the FeB phase and 7.28 wt.% for the Fe_2B phase. If these values are compared with the theoretical weight percentages of element B in the FeB and Fe_2B phases, it is clear that they are relatively close. It should be noted that the EDS method may not accurately detect elements with low atomic numbers, particularly those below eight. As a result, it was concluded that the bilayer (FeB+Fe_2B) were formed on the surface of AISI H13 steel by boronizing process. The results show that elements such as Si, C, and Mo are not soluble, whereas elements like Cr, Mn, V, and Ni are soluble in the boride layer. By observing the change in the amount of element B from the surface to the matrix, it is evident that the amount of element B decreases towards the matrix. It is worth noting that a major drawback of EDS analysis is its reduced accuracy in quantifying elements with low atomic numbers, such as those from Beryllium to Fluorine. Another limitation of EDS analysis is the overlap of X-ray energy peaks between elements, which can cause interference and make it more difficult to distinguish between them. Additionally, matrix effects can be a limitation, as the surrounding material may influence the X-ray emission of the elements, potentially leading to inaccurate measurements. Therefore, the measurement results are often significantly overestimated and cannot be used for accurate determination, such as the boron concentration in the borided layer.

Rodriguez–Castro et al. [27] quantitatively assessed the nickel and chromium levels in (Fe, M)B, $(Fe,M)_2B$, and diffusion zone, where M stands for Cr or Ni. According to their research, (Fe, M)B had an average of 13.5 wt.%Cr and 6.85 wt.% Ni, whereas (Fe, $M)_2B$ had an average of

12.58 wt.% Cr and 6.85 wt.% Ni. However, for the transient zone, the contents of Ni and Cr are quite high compared to the respective contents in the dual boride layer. The EDS analysis was performed by Ozbek and Bindal [28] on the cross-sectional views of AISI M2 steel that had been borided at 850°C for 4 h. They stated that silicon and carbon were ejected toward the substrate and did not dissolve in the boronized layer.

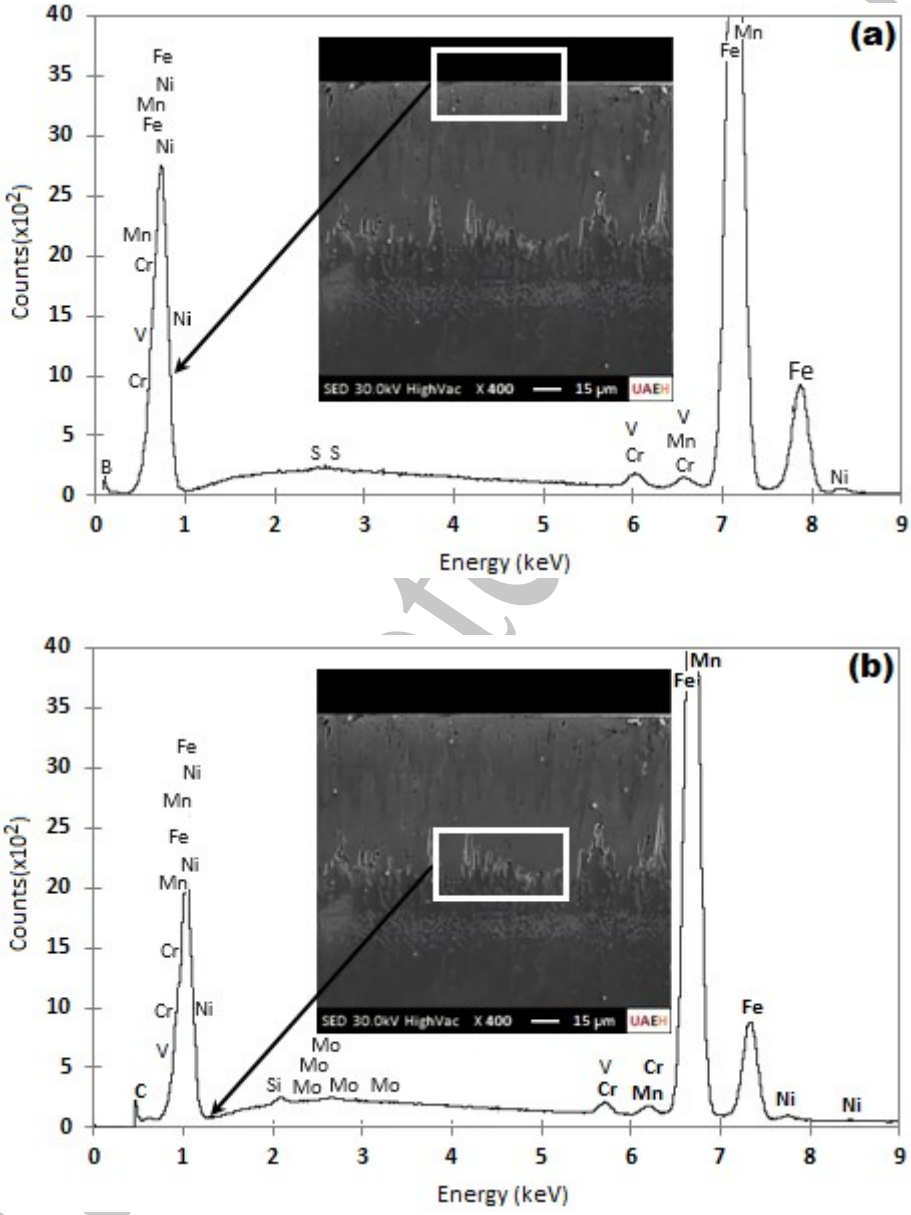

Figure 3. *EDS analyses performed in three regions of the cross-sections of boride layer produced at 1273 K for 8 h, a) In close proximity to the upper surface, b) around the interface area, c) in the untreated zone.*

4.2. XRD analysis

The XRD technique is substantial to identify the crystalline nature of different phases as the iron borides (FeB and Fe_2B) constituting the compact compound layer as well as the probable metal borides in relation to the contents of boride forming-elements present in the chemical composition of treated AISI 304 steel**. Figure 4** provides the XRD patterns of the treated surface of boronized AISI H13 steel at 1273 K for 8 h. The diffraction peaks of iron borides are clearly seen in the XRD patterns confirming the dual nature of obtained boronized layer (FeB and Fe_2B). The presence of chromium (CrB and Cr_2B) was also corroborated because of high contents of chromium in the chemical composition of AISI H13 steel. Moreover, the XRD analysis supported the dual nature of boronized layers as indicated by the SEM results. In comparing our findings with those in the literature, for instance, Gunen et al.[30] reported the presence of CrB and MoB phases in the pack-borided AIS H13 steels. Unlike to our work, the Cr_2B phase was not detected due to the probable use of another powder mixture composed of 95 wt% B_4C and 5 wt.% $NaBF_4$. In another investigation, Zheng et al.[31] found the following phases Fe_2B, FeB, CrB and Cr_2B by XRD analysis when utilizing the powders mixture containing the CeO_2 oxide and such finding are similar to our study despite the use of different powders mixture.

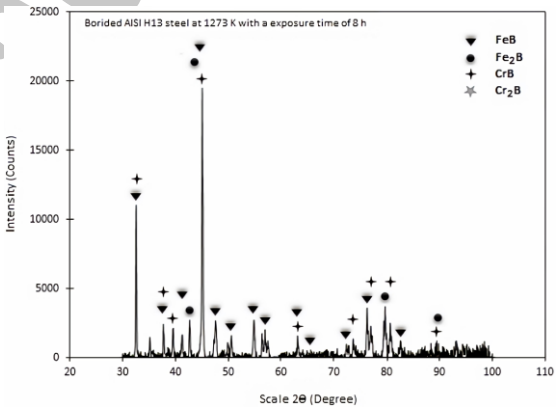

Figure 4. *X-ray diffraction (XRD) diffractogram on the surface of boronized AISI H13 steel at 1273 K during 8 h.*

4.3. Vickers microhardness measurements

Microhardness Vickers tests across the cross-sections of boride layers are required to verify the effectiveness of this boronizing treatment. The process of hardening the surface layers of steel is crucial for enduring all types of wear in mechanical parts operating under extreme working conditions. Consequently, the hardness property is associated with the nature and formation energy of chemical bonds within compounds, such as iron borides (FeB and Fe_2B), or complex borides like (Fe, M)B and (Fe, M)$_2$B, where M represents the alloying element partially soluble in the lattices of iron borides. **Figure 5** gives the SEM micrograph of cross-sections of AISI H13 steel after boronizing at 1273 K for 8 h, illustrating Vickers indentation marks alongside the distribution of microhardness values versus the diffusion depth. The imprints that remained on the cross-sections of the boronized AISI H13 steel at 1273 K for 8 h after applying the Vickers indenter are shown in **Figure 5a**. The variation in the lengths of diagonals on the generated imprints highlights the hardness level reached in each zone (FeB layer, Fe_2B layer and the steel matrix). **Figure 5b** gives the measured microhardness profiles along the cross-section of boronized layer formed on the AISI H13 steel at 1273 K for 8 h. This profile changes in alignment with the boron concentration gradient and steadily diminishes over the diffusion distance. About 10 µm away from the surface, the microhardness value was about 1998 $HV_{0.05}$ and drops to 255 $HV_{0.05}$ when reaching the unaffected steel matrix after the boronizing treatment.

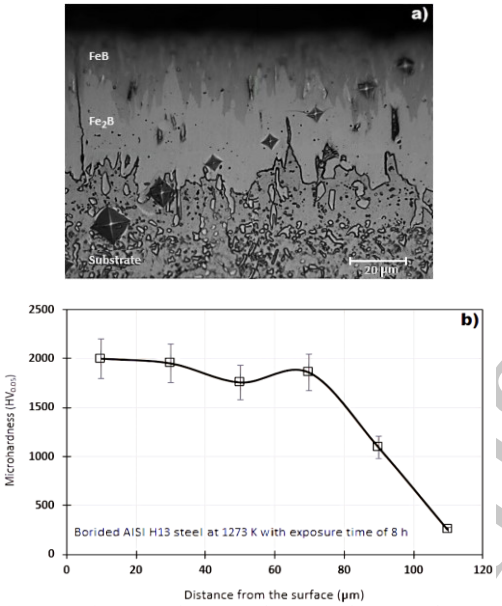

Figure 5. *SEM examination of cross-sectional view of treated AISI H13 steel at 1273 K for 8 h with indentation marks and measurements of microhardness: a) Image of Vickers indentation marks, (b): Measured microhardness-depth profile.*

Taktak [18] developed the Vickers microhardness-depth profiles on the pack-borided AISI 304 steels by taking into account various processing parameters and comparing our results with the literature. He found out that the surface Vickers microhardness averaged 2150 $HV_{0.1}$. The existence of metal borides as precipitates within the dual-phase boronized layers was ascribed to the high value of surface microhardness. It is noted that the Vickers microhardness values measured in this work are consistent with those published in the reference works [18, 29].

4.4. Results from the linear model

The linear kinetic model with new expressions of the two mass balance equations was harnessed to infer the characteristic values of boron diffusion coefficients in both phases (FeB and Fe_2B) by first graphing the time dependencies of layers' thicknesses in the temperature domain of 1123 to 1273 K. **Figure 6** shows the parabolic trend of changes in layers' thicknesses for FeB and (FeB + Fe_2B) with the selected temperature domain with the occurrence of incubation times independent of temperature. In **Table 1** are put together the experimental parabolic growth constants, fitted with Equations (1) and (2), along with the two corresponding incubation periods.

Table 1. *Results of fitting with Equations (1) and (2) with regard to the experimental parabolic growth constants and time incubations.*

T (K)	Experimental constant $2\varepsilon_{FeB}D_{FeB}^{1/2}$ (μm·s$^{-1/2}$)	t_0^{FeB} (s)	Experimental constant $2\varepsilon_{Fe_2B}D_{Fe_2B}^{1/2}$ (μm·s$^{-1/2}$)	$t_0^{Fe_2B}$ (s)	$C_{int}^{Fe_2B}$ (wt.%)
1123	0.07175	3899.4	0.1164	3395.5	8.89
1173	0.1252		0.1979		
1223	0.2088		0.3224		
1273	0.3346		0.5053		

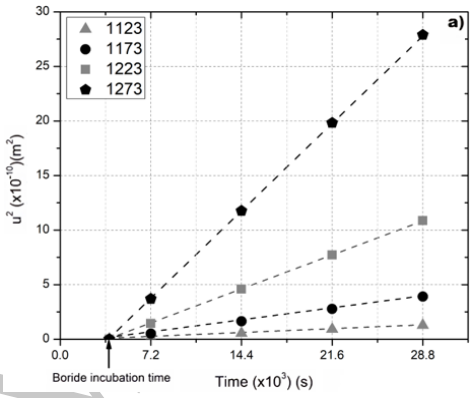

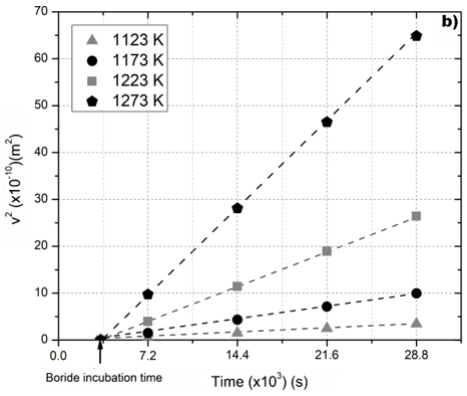

***Figure 6**. Parabolic trends of experimental layers with increasing temperatures: a) FeB layer, b) the bilayer (FeB+ Fe_2B).*

For obtaining the values of diffusion coefficients, it is substantial to search for the two f dimensionless parameters ε_{FeB} and ε_{Fe_2B} by utilizing Equations (19) and (13) for a value of internal boron concentration in Fe_2B estimated as $C_{int}^{Fe_2B}$ =9.89 wt.% B from the equivalence of slopes provided by Equation (11). The calculations yield the two respective values of dimensionless constants ε_{FeB} and ε_{Fe_2B} equal to 0.0638 and 0.0979. Using the data of **Table 1**, the boron diffusion coefficients in each iron boride can be calculated and the calculation results are displayed in **Table 2**.

***Table 2**. Calculated boron diffusion coefficients with the linear model.*

T(K)	D_{FeB} ($m^2 \cdot s^{-1} \times 10^{-12}$)	D_{Fe_2B} ($m^2 \cdot s^{-1} \times 10^{-12}$)
1123	0.32	0.35
1173	0.97	1.02
1223	2.65	2.70

1273	6.72	6.65

The obtained results from **Table 2** were fitted with the Arrhenius-relationships. Therefore, the expressions of boron diffusion coefficients in FeB and Fe_2B were found and given by Equations (20) and (21):

$$D_{FeB} = 4.90 \times 10^{-2} \exp\left(-\frac{240.37 kJ \cdot mol^{-1}}{RT}\right) \quad (20)$$

$$D_{Fe_2B} = 2.33 \times 10^{-2} \exp\left(-\frac{232.62 kJ \cdot mol^{-1}}{RT}\right). \quad (21)$$

where R represents the universal gas constant (8.314 J mol^{-1} K^{-1}), and T is the processing temperature in Kelvin.

Table 3 lists some reported results about the boron activation energies obtained on some boronized steel from the literature [8, 32-40]. It is clearly seen that the published data from different scholars exhibit some intrinsic differences regarding the boriding conditions used and the boriding method. They are mainly influenced by some technological aspects concerning the activation of reactive medium for the boron diffusion. The reported values of activation energies are fundamentally depend upon the calculation method, the chemical composition of the material (steel), the processing parameters (the time duration and the temperature) and so on. To highlight this experimental observations, Keddam et al. [32] managed to surface-harden the AISI 440 C steel with the plasma paste boriding process using a paste containing borax in the range of 700 to 800°C. It is noted that the calculated activation energy for AISI 440 C steel was 134.62 kJ mol^{-1}, which stands as the lowest value among all the data listed in **Table 3**. It is attributed to the utilization of an overactivated medium in conjunction with plasma assistance that enables the

realization of this process at lower temperature (700°C). In a separate study, Ayvaz and Aydin [33] investigated how the growth of layers during the boriding process of 316 L steel is affected by microwave heating. The results obtained from the unconventional heating method enabled a twofold increase in boron diffusion. Campos-Silva et [8] applied the PDCPB process to AISI 8620 steel using two values of polarity inversion half-cycles of 30 s and 50 s, under a current density of 177 mA cm^{-2} . They evaluated the boron activation energies in FeB and Fe_2B as close to 159 and 155 $kJmol^{-1}$, respectively and independently of the value of polarity inversion half-cycles of 30 s and 50 s. It was concluded that this parameters had no effect on the layers' growth kinetics. Albayrak and Vin [34] employed the pack-boriding on DIN St 28 steel with and without mechanical activation as a prior pre-treatment. The Fe_2B layers were obtained in this case without providing the chemical composition of used powders mixture. It was reported that the meachanical activation had no strong effect on calculated boron activations by approximatively 6 %. Kartal et al.[35] treated the AISI T1 steel using the CRTD process in the range of 1123 to 1323 K. The calculated boron activation was estimated as 179.05 $kJmol^{-1}$ with the empirical approach. Such a value of activation was lower compared with the values obtained during the present work for AISI H13 steel because of enhanced mobility of boron within this activated medium attributed to the assistance of electrochemical reactions arising from this CRTD process. In another study, Yu et al. [36] boronized the mild steel employing the spark plasma sintering (SPS) technique. In fact, Introducing SPS to the boriding process has several advantages: including the increase of diffusion rate of boron due to the presence of spark plasma along with the activation of electrical field. The SPS boriding was conducted at temperatures ranging from 700 to 1000 °C for 0.5 h. The estimated boron activation was found to be equal to 145.84 kJ mol^{-1}, highlighting the notable effect of SPS on the kinetics of boriding process. Thus,

the findings [36] indicated that SPS significantly reduced the boron activation energy compared with the conventional powder pack-boriding process [38]. In another investigation, Orihel et al. [37] assessed the boron activation in FeB and Fe_2B for Sleipner steel possessing comparable values with the present study for the AISI H13 steel. Mei et al. [39] performed pack-boronizing on AISI H13 steel using a powder mixture containing rare earth oxides (CeO_2) with varying contents from 2 to 6 wt.%. The aim was to investigate the impact of adding this oxide to the boriding agent on the boronizing kinetics of AISI H13 steel. The results indicated that the addition of rare earth oxide in the powder mixture led to a reduction in boron activation energy and an acceleration of the diffusion rate of boron atoms compared to conventional powder pack-boriding of the same steel, as demonstrated in the present study. Through this study, the obtained values of activation energies in FeB and Fe_2B for AISI H13 steel were attributed to the high proportion of alloying elements, namely Cr and V, inside the substrate. This experimental fact reduces the diffusion rate of boron at deeper distances. The present approach has two limitations during the diffusion process of elemental boron through the surface. In fact, the carbon element present in AISI H13 steel, by forming complex carbides, can interfere with the boron element through a competitive effect, rendering its diffusion more difficult. The precipitation of metal borides as precipitates depletes a certain content of boron, thereby inducing a reduction in the layers' thicknesses. Despite these two limitations, this applied approach is still capable of successfully predicting the boriding kinetics of AISI H13 steel.

Table 3. *Boron Activation energies reported on some steels.*

Steel	Boronizing process	Temperature Range (K)	Activation energy	Calculation Method	Refs.

			(kJ. mol^{-1})		
AISI 440C	Plasma-paste	973-1073 K	134.62 (FeB+ Fe_2B)	Parabolic growth law	[32]
AISI 316L	Powder with microwave heating	1073-1223	(FeB+ Fe_2B) 244.15	Parabolic growth law	[33]
AISI 8620	PDCPB	1123-1223	(FeB) 159, (Fe_2B) 155	Bilayer model	[8]
DIN St 28	Pack boriding with and without mechanical activation (MA)	1023-1123	(Fe_2B) 113.55 and 106.74-108.81 With MA	Empirical relationship	[34]
AISI T1	CRTD	1123-1323	(FeB+Fe_2B) 179.05	Empirical relationship	[35]
Mild	SPS pack-boriding	1073-1273	(FeB+Fe_2B) 145.84	Empirical relationship	[36]
Sleipner	Powder	1173-1323	(FeB) 193.53 (Fe_2B) 179.70	Bilayer model	[37]
AISI 1045	Powder	1123-1273	(Fe_2B) 180	Monolayer model	[38]
AISI H13	Powder	1123-1273	(FeB+Fe_2B) 143.16-160.70 with a variable content of CeO_2	Parabolic growth law	[39]
AISI 304	Powder	1123-1323	(FeB+Fe_2B) 244	Parabolic growth law	[40]

AISI H13	Powder	1123-1273	(FeB) 240.37 (Fe_2B) 232.62	Modified bilayer model	This work

It is possible to determine the need for a straightforward tool to optimize the thicknesses of layers produced during the boronizing process by using the simulation results from the linear model. As a result, we can create common graphs known as contour diagrams (see Figure 7), which express the relationship between the processing parameters (temperature and time duration) and layer thickness. These contour diagrams are intended to assist in selecting the appropriate layer thicknesses to correspond with AISI H13 steel that has been borided for industrial use.

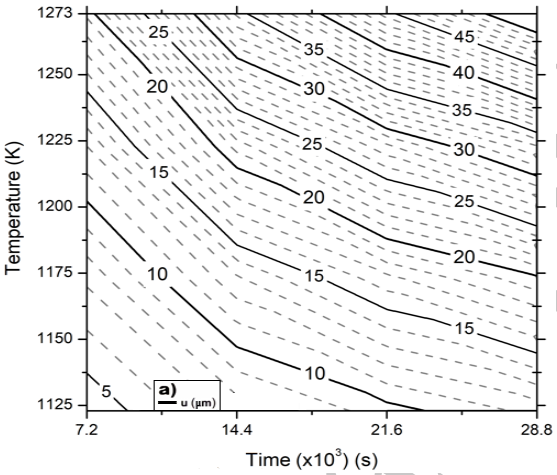

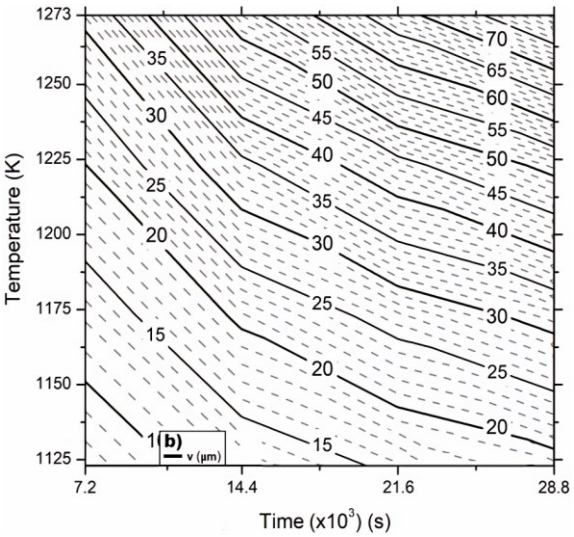

Figure 7. *Iso-thickness diagrams for the borided AISI H13 steel: (a) FeB and (b) FeB + Fe_2B.*

To ascertain the validity of the linear model, two addition processing parameters were considered for this purpose. **Figure 8** shows the SEM cross-sectional views of boride layers obtained at 1323 K for 4.5 and 8.5 h. In Table 4, the experimental layers' thicknesses were compared with the predicted values and a good agreement was achieved between the two sets of data. It is concluded that the model reproduces satisfactory the experimental results in terms of layers' thicknessess.

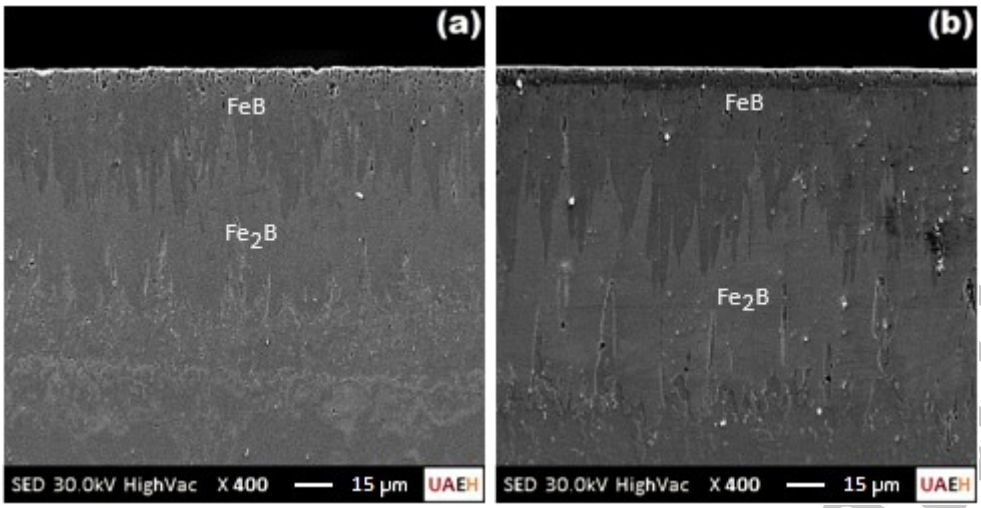

Figure 8. *SEM examination of cross-sectional views of boronized layers obtained at 1323 K for two time durations: a) 4.5 h, b) 8.5 h.*

Table 4. *Comparing the simulated layers' thicknesses with the experimental values from the linear diffusion model for two processing parameters.*

Processing Parameters	u_{exp} (µm)	u_{sim} (µm) using the linear model	v_{exp} (µm)	v_{sim} (µm) using the linear model
1323 K for 4.5 h	53.73 ± 13.5	56.34	89.16 ± 20.3	86.50
1323 K for 8.5 h	85.26 ± 19.1	83.01	124.73 ± 24.7	126.08

.

5. Conclusions

The AISI H13 steel was boronized using the powder method between 1123 and 1273 K for 2-8 h. The findings are summarized in the following points

1. The resulting boronized layers on AISI H13 steel ranged in thickness from 7.18 ± 2.3 to 80.0 ± 19.9 μm and displayed a low toothed shape.

2. The following phases FeB, Fe_2B, CrB and Cr_2B were detected by XRD analysis for all processing parameters.

3. The value of Vickers microhardness measured at 1273 K during 8 h was 1998 $HV_{0.05}$ at a depth of roughly 10 μm below the material surface; in the steel substrate, it attained 255 $HV_{0.05}$.

4. The boron activation energies in both phases 240.37 kJ mol^{-1} for FeB and 232.62 kJ mol^{-1} for Fe_2B were inferred using the linear model. The obtained values of activation energies matched the results found in the literature.

5. Two extra processing parameters (1323 K for 4.5 and 8.5 h) were employed used to validate the current model empirically and the predicted layers' thicknesses were in line the experiments.
6. The contour diagrams were inferred to serve as a valuable tool for selecting the most suitable layer thicknesses that corresponded with the real-world applications of AISI H13 steel.

7. The current approach can be applied to predict the kinetics of interstitial elements (such as B, N and C) through the surfaces of metallic alloys.

Research funding: The work described in this paper was supported by a grant of PRODEP and CONAHCyT México (National Council of Humanities, Science and Technology).

Author Contributions

Visualization, Software and Methodology - original draft, M. Ortiz-Domínguez, Data curation, Formal analysis, Investigation, Á. J. Morales-Robles ; Writing – review & editing, M. Keddam.

Data Availability Statement

Data will be made available on request.

Conflicts of Interest

The authors declare no conflict of interest.

References

[1] F.E. Mariani, G.S. Takeya, L.C. Casteletti, A.N. Lombardi, and G.E. Totten, Kinetics of Layers Produced on Niobium by Salt Bath Boriding, Materials Performance and Characterization, 6 (2017) 467-74. https://doi.org/10.1520/MPC20160095.

[2] Mehmet Tarakci, Yucel Gencer, Adnan Calik, The pack-boronizing of pure vanadium under a controlled atmosphere, Applied Surface Science, 256 (2010) 7612-7618. https://doi.org/10.1016/j.apsusc.2010.06.013.

[3] R. Ribeiro, S. Ingole, M. Usta, C. Bindal, A.H. Ucisik, H. Liang, Tribological investigation of tantalum boride coating under dry and simulated body fluid conditions, Wear, 262 (2007) 1380-1386. https://doi.org/10.1016/j.wear.2007.01.009.

[4] Alaeddine Kaouka, Khedidja Benarous, Electrochemical boriding of titanium alloy Ti-6Al-4V, Journal of Materials Research and Technology, 8 (2019) 6407-6412. ,https://doi.org/10.1016/j.jmrt.2019.10.024.

[5] C.A. Cuao-Moreu, I. Campos-Silva, A.M. Delgado-Brito, E.O. Garcia-Sanchez, A. Juarez-Hernandez, Jose M. Diabb-Zavala, M.A.L. Hernandez-Rodriguez, Effect of laser surface texturing and boriding on the tribocorrosion resistance of an ASTM F-1537 cobalt alloy, Wear, 523 (2023) 204799. https://doi.org/10.1016/j.wear.2023.204799

[6] N. Makuch, M. Kulka, M. Keddam, A. Piasecki, Growth Kinetics, Microstructure Evolution, and Some Mechanical Properties of Boride Layers Produced on X165CrV12 Tool Steel, Materials, 16 (2022) 26. https://doi.org/10.3390/ma16010026

[7] P. Yang, X.C. Wu, Y.A. Min, T.R. Wu, J.Z. Gui, Plasma boriding of high strength alloy steel with nanostructured surface layer at low temperature assisted by air blast shot peening, Surface and Coatings Technology, 228 (2013) 229-233. https://doi.org/10.1016/j.surfcoat.2013.04.033.

[8] M. Olivares-Luna, J.L. Rosales-Lopez, L.E. Castillo-Vela, K.D. Chaparro Pérez, A.M. Delgado-Brito, I. Mejía-Caballero, I. Campos-Silva, Insights on the pulsed-DC powder-pack boriding process: The role of the electric charge on the growth of the boride layer and the semiconductor behavior of the boriding media, Surface and Coatings Technology, 480 (2024) 130588. https://doi.org/10.1016/j.surfcoat.2024.130588.

[9] M. Ortiz-Domínguez, Á.J. Morales-Robles, O.A. Gómez-Vargas, T de J. Cruz-Victoria, Analysis of Diffusion Coefficients of Iron Monoboride and Diiron Boride Coating Formed on the Surface of AISI 420 Steel by Two Different Models: Experiments and Modelling, Materials, 16 (2023) 4801. https://doi.org/10.3390/ma16134801

[10] M. Keddam, J. Peter, Simulating the Growth of Dual-Phase Boride Layer on AISI M2 Steel by Two Kinetic Approaches, Coatings, 11 (2021) 433. https://doi.org/10.3390/coatings11040433

[11] A. Milinović, J. Stojšić, I. Kladarić, B. Matijević, Evaluation of Boride Layers on C70W2 Steel Using a New Approach to Characterization of Boride Layers, Materials, 15 (2022) 3891. https://doi.org/10.3390/ma15113891

[12] Raden Dadan Ramdan, Tomohiro Takaki, Yoshihiro Tomita, Free Energy Problem for the Simulations of the Growth of Fe_2B Phase Using Phase-Field Method, Materials Transactions, 49 (2008) 2625-2631. https://doi.org/10.2320/matertrans.MRA2008158

[13] A.T. Debicha, K. Rayane, O. Allaoui, Modelling Phases Formed during Boriding for Estimation of the Depth of Boron through the Growing in Substrate by the Lattice Boltzmann Method, Defect and Diffusion Forum, 369 (2016) 1662-9507. doi:10.4028/www.scientific.net/DDF.369.177

[14] J.C. Velázquez-Altamirano, I.P. Torres-Avila, G. Teran-Méndez, S.I. Capula-Colindres, R. Cabrera-Sierra, R. Carrera-Espinoza, E. Hernández-Sánchez, A Stochastic Model and Investigation into the Probability Distribution of the Thickness of Boride Layers Formed on Low-Carbon Steel, Coatings, 9 (2019) 756. https://doi.org/10.3390/coatings9110756

[15] M. Bendaoud, M. Keddam, A fuzzy neural network approach for modeling the growth kinetics of FeB and Fe_2B layers during the boronizing process, Matériaux & Techniques, 106 (2018) 603. https://doi.org/10.1051/mattech/2019002

[16] I. Campos, M. Islas, E. González, P. Ponce, G. Ramírez, Use of fuzzy logic for modeling the growth of Fe_2B boride layers during boronizing, Surface and Coatings Technology, 201 (2006) 2717-2723. https://doi.org/10.1016/j.surfcoat.2006.05.016.

[17] N. Vidakis, A. Antoniadis, N. Bilalis, The VDI 3198 indentation test evaluation of a reliable qualitative control for layered compounds, J. Mater. Process. Technol., 143-144 (2003), 481-485. https://doi.org/10.1016/S0924-0136(03)00300-5

[18] S. Taktak, Some mechanical properties of borided AISI H13 and 304 steels, Mater. Des., 28 (2007) 1836-1843. https://doi.org/10.1016/j.matdes.2006.04.017

[19] M. Ortiz-Domínguez, O.A. Gómez-Vargas, M. Keddam, A. Arenas-Flores , J. García-Serrano, Kinetics of boron diffusion and characterization of Fe_2B layers on AISI 9840 steel, Prot. Met. Phys. Chem. S., 53 (2017) 534-547. https://doi.org/10.1134/S2070205117030169

[20] L.G. Yu, X.J. Chen, K.A. Khor, G. Sundararajan, , FeB/Fe_2B phase transformation during SPS pack-boriding: Boride layer growth kinetics, Acta Mater., 53 (2005), 2361-2368. https://doi.org/10.1016/j.actamat.2005.01.043

[21] H. Okamoto, B-Fe (boron-iron), J. Phase Equilibria Diffus., 25 (2004) 297-298. https://doi.org/10.1007/s11669-004-0128-3

[22] R.C. Morón, I. Hernández-Onofre, A.D. Contla-Pacheco, D. Bravo-Bárcenas, I. Campos-Silva, Friction and Reciprocating Wear Behavior of Borided AISI H13 Steel Under Dry and Lubricated Conditions, J. of Materi Eng and Perform, 29 (2020) 4529-4540. https://doi.org/10.1007/s11665-020-04957-w

[23] P. Goeuriot, R. Fillit, F. Thevenot, J.H. Driver, H. Bruyas, The influence of alloying element additions on the boriding of steels, Materials Science and Engineering, 55 (1982) 9-19. https://doi.org/10.1016/0025-5416(82)90078-7

[24] D.N. Tsipas, J. Rus, Boronizing of alloy steels. J Mater Sci Lett, 6 (1987) 118-120. https://doi.org/10.1007/BF01729451

[25] O. Ozdemir, M. Usta, C. Bindal, A. H. Ucisik, Hard iron boride (Fe_2B) on 99.97wt% pure iron, Vacuum, 80 (2006) 1391-1395. https://doi.org/10.1016/j.vacuum.2006.01.022.

[26] S.A. Lysykh, U.L. Mishigdorzhiyn, V.N. Kornopol'tsev, X.Z. He, Yu. P. Kharaev, Structure of Diffusion Layers on Pure Iron at Powder Borocoppering, Tech. Phys., (2024). https://doi.org/10.1134/S1063784224700233

[27] G. A. Rodríguez-Castro, L. F. Jiménez-Tinoco, J. V. Méndez-Méndez, I. Arzate-Vázquez, A. Meneses-Amador, H. Martínez-Gutiérrez, I. Campos-Silva, Damage Mechanisms in AISI 304 Borided Steel: Scratch and Daimler-Benz Adhesion Tests, Materials Research, 18 (2015) 1346-1353. https://doi.org/10.1590/1516-1439.025515

[28] I. Ozbek, C. Bindal, Kinetics of borided AISI M2 high speed steel, Vacuum, 86 (2011) 391-397. https://doi.org/10.1016/j.vacuum.2011.08.004

[29] G.A. Rodríguez-Castro, L.F. Jiménez-Tinoco, J.V. Méndez-Méndez, I. Arzate-Vázquez, A. Meneses-Amador, H. Martínez-Gutiérrez, I. Campos-Silva, Damage Mechanisms in AISI 304 Borided Steel: Scratch and Daimler-Benz Adhesion Tests, Materials Research, 18 (2015) 1346-1353. https://doi.org/10.1590/1516-1439.025515

[30] A. Günen, İ.H. Karahan, M.S. Karakaş, B. Kurt, Y. Kanca, V.V. Çay, M. Yıldız, Properties and Corrosion Resistance of AISI H13 Hot-Work Tool Steel with Borided B_4C Powders. Met. Mater. Int. 26 (2020) 1329-1340. https://doi.org/10.1007/s12540-019-00421-0

[31] Q. Zheng, S. Mei, Z. Xiao, Z. Hu, Z. Chen, Q. Xu, A. Guryev, B. Lygdenov, Tribological, oxidation and corrosion properties of ceramic coating on AISI H13 steel by rare earth-Cr composite boronizing, Ceramics International, 50 (2024) 8760-8776.https://doi.org/10.1016/j.ceramint.2023.12.193.

[32] M. Keddam, R. Chegroune, M. Kulka, D. Panfil, S. Ulker, S. Taktak, Characterization and diffusion kinetics of the plasma paste borided AISI 440C steel, T. Indian I. Metals, 70(2017) 1377-1385. https://doi.org/10.1007/s12666-016-0934-4

[33] S.I. Ayvaz, I. Aydin, Effect of the Microwave Heating on Diffusion Kinetics and Mechanical Properties of Borides in AISI 316L, Trans Indian Inst Met., 73 (2020) 2635-2644. https://doi.org/10.1007/s12666-020-02072-x

[34] M.G. Albayrak, E. Evin, A Different Approach: Effect of Mechanical Alloying on Pack Boronizing, J. of Materi Eng and Perform (2023). https://doi.org/10.1007/s11665-023-09004-y

[35] G.K. Sireli, H. Yuce, M. Arslan, M. Karimzadehkhoei, S. Timur, Improving the Surface Performance of Discarded AISI T1 Steel by Cathodic Reduction and Thermal Diffusion-Based Boriding. J. of Materi Eng and Perform, 32 (2023), 9504-9514. https://doi.org/10.1007/s11665-023-07817-5

[36] L.G Yu, K.A Khor, G Sundararajan, Boriding of mild steel using the spark plasma sintering (SPS) technique, Surf. Coat. Technol., 157 (2002) 226-230, https://doi.org/10.1016/S0257-8972(02)00134-2.

[37] P. Orihel, J. Ptačinová, P. Gogola, M. Keddam, P. Jurči, Pack-boriding of Sleipner steel: microstructure analysis and kinetics modeling Materials Testing, 66 (2024) 43-55. https://doi.org/10.1515/mt-2023-0331

[38] J. Zuno-Silva, M. Ortiz-Domínguez, M. Keddam, M. Elias-Espinosa, O. Damián-Mejía, E. Cardoso-Legorreta, M. Abreu-Quijano, Boriding kinetics of Fe_2B layers formed on AISI 1045 steel, J. Min. Metall. Sect. B-Metall., 50 (2014) 101-107. https://doi.org/10.2298/JMMB140323019Z

[39] S. Mei, Y. Zhang, Q. Zheng, Y. Fan, B. Lygdenov, A. Guryev, Compound Boronizing and Its Kinetics Analysis for H13 Steel with Rare Earth CeO_2 and Cr_2O_3, Applied Sciences, 12 (2022) 3636. https://doi.org/10.3390/app12073636

[40] P. Topuz, B. Çiçek, O. Akar, Kinetic ınvestigation of AISI 304 stainless steel boronized in ındirect heated fluidized bed furnace, J. Min. Metall. Sect. B-Metall., 52 (2016) 63-68. https://doi.org/10.2298/JMMB150301007T

Figure captions

Figure 1. *Schematic depiction of linear profiles of boron element when creating the bilayer (FeB/ Fe_2B).*

Figure 2. *SEM examinations of the cross-sections of boronized layers on AISI H1 steel at 1273 K for increasing time durations : a) 1273 K for 2 h, b) 1273 K for 4 h, c) 1273 K for 6 h and d) 1273 K for 8 h.*

Figure 3. *EDS analyses performed in three regions of the cross-sections of boride layer produced at 1273 K for 8 h, a) In close proximity to the upper surface, b) around the interface area, c) in the untreated zone.*

Figure 4. *X-ray diffraction (XRD) diffractogram on the surface of boronized AISI H13 steel at 1273 K during 8 h.*

Figure 5. *SEM examination of cross-sectional view of treated AISI H13 steel at 1273 K for 8 h with indentation marks and measurements of microhardness: a) Image of Vickers indentation marks, (b): Measured microhardness-depth profile.*

Figure 6. *Parabolic trends of experimental layers with increasing temperatures: a) FeB layer, b) the bilayer (FeB+ Fe_2B).*

Figure 7. *Iso-thickness diagrams for the borided AISI H13 steel: (a) FeB and (b) FeB + Fe_2B.*

Figure 8. *SEM examination of cross-sectional views of boronized layers obtained at 1323 K for two time durations: a) 4.5 h , b) 8.5 h.*

Table captions

Table 1. *Results of fitting with Equations (1) and (2) with regard to the experimental parabolic growth constants and time incubations.*

Table 2. *Calculated boron diffusion coefficients with the linear model.*

Table 3. *Boron Activation energies reported on some steels.*

Table 4. *Comparing the simulated layers' thicknesses with the experimental values from the linear diffusion model for two processing parameters.*